Tissue Engineering

Tissue Engineering Manuscript Central: http://mc.manuscriptcentral.com/liebert/ten

Prediction of the optimal mechanical properties for a scaffold used in osteochondral defect repair

Journal:	*Tissue Engineering*
Manuscript ID:	TEN-05-0410.R1
Manuscript Type:	Original Article
Date Submitted by the Author:	n/a
Complete List of Authors:	Kelly, Daniel; University of Dublin, Trinity College, Mechanical Engineering Prendergast, Patrick; University of Dublin, Trinity College, Mechanical Engineering
Keyword:	Mesenchymal Stem Cells < Fundamentals of Tissue Engineering, Computer-Aided Tissue Design < Enabling Technologies, Cartilage < Tissue Engineering Applications, Cell Differentiation < Fundamentals of Tissue Engineering, Mechanical Effects on Cells and Tissues < Fundamentals of Tissue Engineering

Prediction of the optimal mechanical properties for a scaffold used in osteochondral defect repair

Daniel J. Kelly, Ph.D. and Patrick J. Prendergast, Ph.D.

Centre for Bioengineering, Department of Mechanical and Manufacturing Engineering, Trinity College, Dublin, Ireland.

Address correspondence to:

Dr. Daniel Kelly

Mailing Address:

Centre for Bioengineering,

Department of Mechanical Engineering,

Trinity College Dublin,

Dublin 2,

Ireland.

Contact Information:

Tel: +353-1-6083947 (Daniel Kelly); +353-1-6083393 (Patrick Prendergast).

Fax: +353-1-6795554 (Daniel Kelly); +353-1-6795554 (Patrick Prendergast).

Email: kellyd9@tcd.ie (Daniel Kelly); pprender@tcd.ie (Patrick Prendergast).

Abstract

The optimal mechanical properties of a scaffold to promote cartilage generation in osteochondral defects *in vivo* are not known. During normal daily activities cartilage is subjected to large cyclic loads that not only facilitate nutrient transport and waste removal through the dense tissue but also act as a stimulus to the chondrocytes. In contrast, cartilage tissue is commonly engineered *in vitro* in a static culture and hence, in many cases, the properties of scaffolds have been tailored to suit this *in vitro* environment. In this study, a mechano-regulation algorithm for tissue differentiation has been used to determine the influence scaffold material properties on chondrogenesis in a finite element model of an osteochondral defect. It is predicted that increasing the stiffness of the scaffold increases the amount of cartilage formation and reduces the amount of fibrous tissue formation in the defect, but this only holds true up to a certain threshold stiffness above which the amount of cartilage formed is reduced. Reducing the permeability of the scaffold was also predicted to be beneficial. Considering a non-homogenous scaffold, an optimal design was determined by parametrically varying the mechanical properties of the scaffold through its depth. The Young's modulus reduced non-linearly from the superficial region through the depth of the scaffold, while the permeability of the scaffold was lowest in the superficial region. As tissue engineering moves from a science towards a product, engineering design becomes more relevant, and predictive models such as that presented here can provide a scientific basis for design choices.

Introduction

The optimal properties for a scaffold used in cartilage tissue engineering have traditionally been defined in terms of those properties which will optimise tissue formation *in vitro*. Besides ensuring the obvious need for biocompatibility, significant effort has also gone into developing scaffolds that are both highly porous and permeable, facilitating a homogenous cell seeding, increased cell attachment and diffusion of nutrients and growth factors to the cells throughout the scaffold. Scaffolds fabricated from synthetic biodegradable polymers such as poly-L-lactic acid (PLA), polyglycolic acid (PGA) [1,2] and copolymer poly(L-lactic acid-glycolic acid) (PLGA) [3], as well as gels such as collagen [4], alginate [5] and agarose [6] possess many of these properties and have been shown to support, to differing degrees, the chondrogenic phenotype and proliferation *in vitro*, and the synthesis of collagen type II and proteoglycan. Furthermore when used to treat osteochondral defects *in vivo*, such cell seeded scaffolds have improved the quality of the repair tissue compared to untreated controls [7,8,9,10,11]. However the repair tissue is still both biomechanically and biochemically inferior to normal articular cartilage [7,11], and long term results have been mixed, with for example, morphological stable hyaline cartilage reported in approximately half all defects 18 months after implantation [8]. It would seem therefore that even if a scaffold or gel promotes chondrogenesis *in vitro* is does not necessarily produce a functional repair tissue *in vivo*.

More recently, efforts have been made to improve the quality of the repair tissue by attempting to create a more functional engineered tissue or scaffold prior to implantation. Schaefer *et al*. [12] implanted a tissue engineered cartilage construct,

Mary Ann Liebert, Inc.,140 Huguenot Street, New Rochelle, NY 10801

generated by bioreactor culture of chondrocytes seeded onto polyglycolic acid scaffolds and combined with an osteoinductive support, into large osteochondral defects in the femoropatellar grove of adult rabbits. The engineered cartilage withstood physiological loading and remodelled into osteochondral tissue with characteristic architectural features and Young's moduli approaching that of normal articular cartilage 6 months after implantation. Niederauer *et al.* [9] examined how the mechanical and physical properties of a *multiphase* scaffold (scaffold with different cartilage and bone phases) can influence the cartilage healing response in osteochondral defects. A scaffold with a stiffer cartilage phase was ranked higher than a control scaffold in high weight-bearing regions. Interestingly this study showed that the addition or omission of cells to the scaffold prior to implantation had little effect on the quality of repair.

Based on these and other studies, it would seem that the mechanical properties of the scaffold or engineered tissue prior to implantation into an osteochondral defect are key determinants of its success. The mechanical properties of a scaffold will influence the mechanical environment of the seeded cells. We hypothesize that this in turn can influence the differentiation pathway of the cell, for example by encouraging the differentiation of undifferentiated mesenchymal stem cells towards the chondrogenic lineage, or by inducing the dedifferentiation of a mature chondrocyte towards a fibroblast-like cell. Furthermore the mechanical environment can be expected to influence cell viability [13]. Previously a mechano-regulation model has been developed which relates the differentiation of cells of the mesenchymal lineage to their mechanical environment [14], and used to successfully predict the patterns of tissue differentiation during fracture healing [15], around orthopedic implants [16] and during spontaneous

osteochondral defect repair [17]. The idea that mechanical stimuli influenced tissue differentiation began with Pauwels [18], who recognized that physical factors cause stress and deformation of the mesenchymal stem cells, and that these stimuli could determine cell differentiation pathways. This concept was further developed by Carter *et al* [19] to analyze patterns of tissue differentiation during fracture healing, and more recently new hypotheses have been proposed by a number of different authors [20, 21, 22, 23]. In this paper we will attempt to use such a model [17] to determine the optimal mechanical properties for a scaffold used in osteochondral defect repair to promote the differentiation of mesenchymal stem cells towards the chondrogenic phenotype, and hence produce a functional hyaline-like repair tissue.

Methods

In most tissue engineering applications, whether by design or not, the scaffold plays a key role in regulating the mechanical environment of the cell. The mechanobiological processes of the cell are in turn regulated by this mechanical environment. In a previous paper [17], a model of mechano-regulated stem cell differentiation by strain and fluid flow, which was initially conceived by comparing the magnitude of these biophysical stimuli to patterns of tissue differentiation around a micro-motion device implanted into the chondyles of dogs [24, 14], was further developed to include cellular events not considered previously but which may be important for realistic simulation of tissue engineering strategies for connective tissue repair. Briefly, in this model stem cells can differentiate into cells of different phenotypes denoted i (i.e. fibroblasts, chondrocytes or osteoblasts) that produce different connective tissues denoted j (i.e. fibrous tissue,

cartilage or bone). The dispersal of cells of a particular phenotype *i* throughout a given region can be simulated by assuming the cell population to be described by diffusive, proliferative and apoptotic processes as follows:

$$\underbrace{\frac{dn^i}{dt}}_{\text{rate of change in number of cells}} = \underbrace{D^i \nabla^2 n^i}_{\text{cell dispersal modeled by diffusion}} + \underbrace{P^i(S)n^i}_{\text{proliferation as a function of a stimulus}} - \underbrace{K^i(S)n^i}_{\text{apoptosis as a function of a stimulus}} \quad \text{, (Eqn. 1)}$$

where n^i denotes the number of cells of a particular cell phenotype *i*, D^i the diffusion coefficient to model dispersal (by proliferation and migration) for cell phenotype *i*, $P^i(S)$ is a proliferation rate and $K^i(S)$ is an apoptosis (death) rate for cell *i* as a function of a biophysical stimulus *S*. Eqn. 1 assumes that cell movement can be described using a diffusion equation whereby cell dispersal occurs from regions of high cell density to low cell density. As a first step, a simple quadratic relationship was assumed between cell proliferation P^i and cell death K^i and the magnitude of the biophysical stimulus *S* such that

$$P^i(S)n^i - K^i(S)n^i = a_i + b_i S_o + c_i S_o^2, \qquad \text{(Eqn. 2)}$$

where S_o is the octahedral shear strain. Eqn. 2 assumes a non-linear relationship exists between mitosis/cell death and the magnitude of strain experienced by cells. As cells disperse throughout the repair tissue, they are hypothesized to differentiate depending on the magnitude of a biophysical stimulus, see Fig. 1. Following previous work [14, 15, 16, 17], the biophysical stimulus for tissue differentiation is taken to be a function of the octahedral shear strain γ and interstitial fluid flow v in the extracellular environment of the cells according to:

$$S = \frac{\gamma}{a} + \frac{v}{b}. \qquad \text{(Eqn. 3)}$$

Cells can differentiate into the following cell phenotypes and synthesise a new tissue type based on the value of S:

$p_{\text{resorbtion}} < S < p_{\text{mature}}$ osteoblast: mature woven bone

$p_{\text{mature}} < S < 1$ osteoblast: immature woven bone

$1 < S < q$ chondrocyte: cartilage

$S < q$ fibroblast: fibrous connective tissue (Eqn. 4)

where $p_{\text{resorbtion}}$ (0.01), p_{mature} (0.53) and q (3) represent boundaries of the mechano-regulation diagram for tissue differentiation. In the region $0 < S < p_{\text{resorbtion}}$ bone resorbtion occurs. The different ranges of S taken to regulate tissue differentiation are based upon the previous work of Huiskes *et al.* [16], who used these ranges of values to successfully predict the patterns of tissue differentiation observed experimentally by Søballe *et al.* [24]. In these animal experiments [24], the gap tissue surrounding a force-actuated piston implant gradually differentiated from granulative to fibrous, to cartilaginous and finally to bone tissue. Prendergast *et al.* [14] determined that the magnitudes of strain and fluid velocity within the gap tissue reduced during differentiation due to tissue maturation, and hypothesized that this was regulating the differentiation process. By encapsulating this concept into a computer simulation model, and using the range of values for S given above, Huiskes *et al.* [16] observed that the predicted patterns of tissue differentiation coincided with those found experimentally.

The biophysical stimulus S is determined using a linear poroelastic axi-symmetric finite element model (Diana, TNO, Delft, The Netherlands) of a large osteochondral defect (radius = 7 mm) within the chondyle of the femur, see Fig. 2. The material properties used for each tissue type are listed in Table 1. The meniscus is modelled as

transversely isotropic with a higher stiffness in the circumferential direction (E_1, E_2 = 0.5 MPa; E_3 = 100 MPa; ν_{12} = 0.5; ν_{13} = 0.0015). A ramp loading of 800 N is applied to the femur over a period of 0.5 seconds. Initially the osteochondral defect was assumed to be cell free and filled with a granulation tissue. As healing progresses cells will invade the defect from the bone marrow, differentiate and synthesize extracellular matrix that alters the mechanical properties of the repair tissue. This process is modelled by iteratively updating the mechanical properties within the finite element model depending on the number and phenotype of the cells within the defect. Within each iteration, the distribution of cells through the defect is determined by solving Eqn. 1. The material properties of every element in the finite element model are then recomputed using a rule of mixtures that accounts for both the number and phenotype of cells within each element [17]. A new iteration then begins to re-calculate the biophysical stimulus S based on the new material properties, cell numbers and phenotypes.

To study the influence of a scaffold on osteochondral defect repair, two different types of scaffold were incorporated into the finite element model of the defect:

(i) A homogenous scaffold modeled as a linear poro-elastic material, where both the Young's modulus (E) and the permeability (k) of the scaffold were varied parametrically to assess the influence of scaffold material properties on defect repair, see Table 2.

(ii) An inhomogeneous scaffold modeled with two distinct phases, a chondral phase and a bone phase. The mechanical properties of the chondral phase are varied from the superficial layer through the depth of the scaffold. In this model, the Young's modulus of the chondral phase of the scaffold decreases

from 60 MPa in the superficial layer to 10 MPa in the base of the chondral phase of the scaffold. The permeability of the chondral phase increases from 1e-16 m^4/Ns in the superficial layer to 2e-15 m^4/Ns in the base of the chondral phase of the scaffold. The bone phase of the scaffold has a uniform stiffness of 50 MPa and a permeability of 2e-15 m^4/Ns. To establish an optimal scaffold design, both the Young's modulus and the permeability were then varied between these upper and lower limits throughout the depth of the chondral phase of the scaffold until the amount of fibrous tissue formation predicted was minimized.

In both models the other material properties for the scaffold (Poisson's ratio, porosity, solid and fluid compression modulus) were set to that of granulation tissue. In the simulation, the mechanical properties of each element in the defect remain those of the scaffold material until the properties of the regenerating tissue within the element exceeds (or are less than in the case of permeability and porosity) that of the scaffold.

Results

In the absence of a scaffold (spontaneous repair), the simulations show that, initially, the defect is partially shielded from the load by the adjacent intact cartilage, and the stimulus within the defect is low. This low level of mechanical stimuli favours osteogenesis. As the repair tissue begins to stiffen, it begins to support load, and chondrogenesis is favoured within the centre of the defect. Fibrous tissue is predicted to form at the articular surface due to the high magnitudes of strain and fluid flow in this region of the repairing tissue (Fig. 3a). After some time, increased bone formation is predicted to occur by

Mary Ann Liebert, Inc.,140 Huguenot Street, New Rochelle, NY 10801

endochonrdal ossification, and regions of cartilage begin to differentiate into fibrous tissue leading ultimately to a reduction in the amount of cartilage within the defect.

The predicted patterns of tissue differentiation after implantation of a homogenous scaffold (E = 10 MPa, permeability = 1e-4 m^4/Ns) are noticeably different to that predicted during spontaneous repair without a scaffold (compare Fig. 3a with Fig. 3b). The scaffold is predicted to support early chondrogenesis, with the chondral region of the defect consisting primarily of immature cartilage tissue (iteration 5). Increased cartilage formation is predicted as the simulation of defect repair progresses, with a significantly greater proportion of the defect consisting of cartilage tissue (iteration 10). Endochondral ossification is observed (iteration 20) that continues until the bony region of the defect consists primarily of bone, apart from a pocket of cartilage tissue persisting in the upper corners of the defect. A remarkably uniform band of fibrous tissue persists at the articular surface; however the remainder of the chondral part of the defect consists nearly exclusively of cartilage tissue.

During spontaneous repair (no scaffold), significant cell death was predicted at the articular surface due to the high stimulus (strain) there. Implanting a scaffold was predicted to prevent this cell death due to the lower strains experienced by cells in the presence of a scaffold (Fig. 4).

Reducing the modulus of the scaffold to 1 MPa resulted in increased bone formation, reduced cartilage formation and increased fibrous tissue formation, similar, in fact, to that observed in an empty defect (Fig. 5). Interestingly increasing the modulus of the scaffold to 50 MPa was predicted to have a similar effect on the amounts of each tissue type within the defect as reducing the modulus to 1 MPa, with increased amounts

of bone and fibrous tissue formation and reduced amounts of cartilage formation predicted to form within the defect; however the *patterns* of tissue differentiation predicted using the 1 MPa vs. the 50 MPa scaffolds were different, with regions of cartilage predicted to persist in the base of the defect with the stiffer scaffolds (Fig. 6).

The type of repair predicted when the permeability of the scaffold is reduced to 5e-15 m^4/Ns is similar to that predicted with the baseline permeability (1e-14 m^4/Ns). When the permeability is reduced to 1e-15 m^4/Ns, the increased cartilage formation that is usually predicted during the early stages of healing is not observed, and instead larger amounts of bone formation occurs primarily from direct intramembranous ossification with little or no endochondral bone formation (Fig. 7). Down to a certain threshold value (1e-15 m^4/Ns), reducing the permeability is also predicted to reduce the amount of fibrous tissue within the defect, below which fibrous tissue formation either levels off or increases (Fig. 7).

It is predicted that the amount of fibrous tissue can be reduced to a very small percentage (~ 1%) of the repair tissue by implanting an *optimized* inhomogeneous scaffold. The Young's modulus of such an *optimized* scaffold is predicted to be one whose modulus reduces non-linearly from 60 MPa in the superficial layer to 10 MPa in the base of the chondral phase of the scaffold, while the permeability of the chondral phase increases non-linearly from 1e-16 m^4/Ns in the superficial layer to 2e-15 m^4/Ns in the base of the chondral phase of the scaffold, as depicted in Fig. 8. With this optimized scaffold, primarily cartilage tissue formation is predicted in the chondral region of the osteochondral defect, and primarily bone tissue is predicted to form in the bony region of

the defect (Fig. 9). To see the effectiveness of the inhomogeneous scaffold, compare Fig. 9 with Fig. 3.

Discussion

At present, a predominantly experimental approach is taken in tissue engineering of cartilage. While this is certainly appropriate, a broader engineering methodology also requires the development of predictive models which can be used for design purposes. The computational model presented in this paper offers a framework for such an engineering design. However it is based on a number of simplifications. These include the assumption that cell movement can be described using a diffusion equation [25], that a non-linear relationship exists between mitosis/cell death and the magnitude of strain experienced by cells [17], and that tissue differentiation is regulated by a combination of the magnitude of octahedral shear strain and fluid flow within the tissue [14]. The finite element model of the osteochondral defect is also based on a considerable simplification, in particular the constitutive models chosen for the soft tissues and the axisymmetric model used to represent the geometry of the knee. Future models will need to take account of non-linear, inhomogeneous nature of soft tissues such as cartilage [26, 27]. We also introduce the concept of modeling a scaffold inside an osteochondral defect. We made no attempt to account for the fact that the scaffold may degrade over time, but this could be easily accounted for if required. The bulk properties of any one element in the defect remain that of the scaffold until the point in the simulation in which the properties of the regenerating tissue exceeds (or are less than in the case of permeability and porosity) that of the scaffold. It should also be noted that the mechanical properties of the

scaffold, particularly the permeability, may alter by filling with debris tissue after implantation. Another potentially important addition to the model would be to account for the influence of nutrient transport and growth factors on the tissue differentiation process [28]. For example, growth factors and dynamic loading have been shown to have synergistic effects in cartilage bioreactors studies [29]. Despite these limitations the model has successfully predicted many features of the tissue differentiation process observed during spontaneous osteochondral defect repair [30, 31]. For example, Shapiro *et al.* [30] observed bone formation through both endochondral and direct intramembranous ossification in the base of the defect, cartilage formation in the centre of the defect, and fibrous tissue formation superficially. This pattern of repair is also observed in the model. This provides evidence to confirm the hypothesis of mechano-regulated tissue differentiation on which the model is based. Geris *et al.* [32] also report that predicted patterns of tissue differentiation around loaded bone chambers show a qualitative agreement with the results of rabbit experiments, providing further independent corroboration for this mechano-regulation hypothesis. The evidence is by no means conclusive, and the model will have to be continuously tested by attempting to simulate tissue differentiation in different circumstances; however it does suggest that the mechano-regulation model can be used as a tool in evaluating tissue-engineering strategies.

The primary function of a scaffold in cartilage tissue engineering has traditionally been as a device to maintain the chondrogenic phenotype and provide a three dimensional structure for cells to lay down new matrix. Numerous types of scaffolds have successfully exhibited these properties *in vitro*. While it seems that implanting such a scaffold into an

osteochondral defect improves the quality of healing over the spontaneous repair process, the exact mechanical properties that such a scaffold should possess have yet to be elucidated. If improved repair is defined as:

(i) maximizing the amount of bone tissue forming in the bony part of the defect, and

(ii) maximizing the cartilage tissue forming in the chondral part of the defect, which equates to minimizing fibrous tissue formation and producing a uniformly thick layer of cartilage repair tissue, and

(iii) preventing cell death within the defect,

then these simulations suggest that a scaffold must have a certain minimum stiffness to reduce fibrous tissue formation within the defect. However if the scaffold is too stiff the amount of fibrous tissue formation predicted to form within the defect starts to increase (see Fig. 10), due in part to an increase in the magnitude of fluid flow within the defect, leading to a situation where the stimulus for fibrous tissue formation is increased due to increases in fluid flow. Increasing the stiffness of the scaffold also reduces the thickness of the repair cartilage due to further progression of the osseous front – from these results it would seem that an optimal stiffness for a scaffold should exist.

It was found that reducing the permeability of the scaffold would further reduce the amount of fibrous tissue formation within the defect; in this respect reducing scaffold permeability is a benefit. However if the permeability of the scaffold is too low the amount of fibrous tissue formation within the defect is again predicted to increase (see Fig. 9). In this case, reducing the permeability of the scaffold beyond a certain threshold value (1e-15 m^4/Ns) leads to a slight increase in the stimulus for fibrous tissue formation

by increasing the octahedral shear strain in the superficial region of the defect. This increase in strain also leads to increased cell death at the articular surface. Preventing this fibrous tissue formation superficially, and any subsequent cell death, by implanting a scaffold with the appropriate mechanical properties would appear beneficial in preventing long-term failure of the repair tissue.

We propose that the *optimal* scaffold for osteochondral defect repair will have depth-dependant mechanical properties, with a Young's modulus that reduces in magnitude and a permeability that increases in magnitude from the superficial zone through the depth of the chondral phase of the scaffold (Fig. 8). Mechanical testing has shown that the tensile modulus of normal articular cartilage can be 6-20 times greater in the superficial zone of the tissue than in the middle-deep zone of the tissue [33], and that the permeability of the tissue increases between the superficial and mid zone [34]. This study therefore comes to what may seem an obvious conclusion regarding the design of scaffolds for osteochondral defect repair - that the mechanical properties of the scaffold should mimic to some extent the mechanical properties of the extracellular matrix of the tissue it intends to replace. The optimized scaffold proposed in this paper can be seen as a template for future scaffold design, with the mechanical properties of the scaffold also depending on specific factors such as the size and weight of the patient and the location of the defect. In the future it may be possible to design patient-specific scaffolds based on computer simulations of the kind presented in this paper. The advantage of such an approach has been highlighted by Semple *et al.* [35], who argue that one of the key enabling features of computational methods in tissue engineering is to expedite the

testing of new constructs and scaffolds and to develop strategies to identify optimal therapy for individual patients.

The properties of the optimized scaffold proposed in this paper are very different to many of the scaffolds that are currently been evaluated for cartilage repair. It is suggested that many of these scaffolds have been designed to promote cartilage formation in a static culture, which is obviously very different to the environment *in vivo,* and therefore the suitability of such scaffolds for cartilage repair *in vivo* has yet to be fully elucidated. Similarly the design of scaffold proposed in this paper is to promote chondrogenesis *in vivo,* and therefore such a scaffold may prove unsuccessful in the *in vitro* setting, due for example, to limitations in nutrient diffusion in such a low permeability scaffold. A more suitable *in vitro* study to access the potential of such a scaffold may be to provide physiological loading using a suitable bioreactor.

In conclusion, a mechano-regulation model has been used to predict the optimal mechanical properties for a scaffold used in osteochondral defect repair. Implanting such a scaffold into an osteochondral defect is predicted to minimize the amount of fibrous tissue formation. This paper highlights the potential usefulness of predictive models in engineering replacement tissues.

Acknowledgements

This work was funded by the European Union under the BITES project (Contract #: QLK3-CT-1999-00559).

References

1. Freed, L.E., Marquis, J.C., Nohria, A., Emmanual, J., Mikos, A.G., Langer, R. Neocartilage formation in vitro and in vivo using cells cultured on synthetic biodegradable polymers. J. Biomed. Mater. Res. **27**, 11, 1993.
2. Grande D.A., Halberstadt C., Naughton G., Schwartz R., Manji R. Evaluation of the matrix scaffolds for tissue engineering of articular cartilage grafts. J. Biomed. Mater. Res. **34**, 211, 1997.
3. Rahman, M.S., Tsuchiya, T. Enhancement of chondrogenic differentiation of human articular chondrocytes by biodegradable polymers. Tissue Eng. **7**, 781, 2001.
4. Kimura, T., Yasui, N., Ohsawa, S., Ono, K. Chondrocytes embedded in collagen gels maintain cartilage phenotype during long-term cultures. Clin. Orthop. Relat. Res. **186**, 231, 1984.
5. Van Susante, J.L.C., Buma, P., Van Osch G.J.V.M, Versleyen D., Van der Kraan, P.M., Van der Berg, W.B., Homminga, G.N. Culture of chondrocytes in alginate and collagen carrier gels. Acta. Orthop. Scand. **66**, 549, 1995.
6. Benya, P., Schaffer, J. Dedifferentiated chondrocytes reexpress the differentiated collagen phenotype when cultured in agarose gels. Cell **30**, 215, 1982.
7. Wakitani, S., Goto, T., Pineda, S.J. Mesenchymal cell-based repair of large, full-thickness defects of articular cartilage. J. Bone Joint Surg. **76-A**, 579, 1994.
8. Rahfoth, B., Weisser, J., Sternkopf, F., Aigner, T., von der Mark, K. Transplantation of allograft chondrocytes embedded in agarose gel into cartilage defects in rabbits. Osteoarthritis Cartilage **6**, 50, 1998.

9. Niederauer, G.G., Slivka, M.A., Leatherbury, N.C., Korvick, D.L., Harroff, H.H., Ehler, W.C., Dunn, C.J., Kieswetter, K. Evaluation of multiphase implants for repair of focal osteochondral defects in goats. Biomaterials **21**, 2561, 2000.

10. Wakitani, S., Goto, T., Young, R.G., Mansour, J.M., Goldberg, V.C., Caplan, A.C. Repair of large full-thickness articular cartilage defects with allograft articular chondrocytes in a collagen gel. Tissue Eng. **4**, 429, 1998.

11. Liu, Y., Chen, F., Liu, W., Cui, L., Shang, Q., 2002. Repairing large porcine full-thickness defects of articular cartilage using autologous chondrocyte-engineered cartilage. Tissue Eng. **8**, 709, 2002.

12. Schaefer, D., Martin, I., Jundt, G., Seidel, J., Heberer, M., Grodzinsky, A., Bergin, I., Vunjak-Novakovic, G., Freed, L.E. Tissue-engineered composites for the repair of large osteochondral defects. Arthritis Rheum. **46**, 2524, 2002.

13. Loening, A.M., James, I.E., Levenston, M.E., Badger, A. M., Frank, E. H., Kurz, B., Nuttall, M. E., Hung, H. H., Blake, S. M., Grodzinsky, A. J., Lark, M. W. Injurious mechanical compression of bovine articular cartilage induces chondrocyte apoptosis. Arch. Biochem. Biophys. **381**, 205, 2000.

14. Prendergast, P.J., Huiskes, R., Søballe, K. Biophysical stimuli on cells during tissue differentiation at implant interfaces. J. Biomech. **30**, 539, 1997.

15. Lacroix, D., Prendergast, P.J. A mechano-regulation model for tissue differentiation during fracture healing: analysis of gap size and loading. J. Biomech. **35**, 1163, 2002.

16. Huiskes, R., van Driel, W.D., Prendergast, P.J., Søballe, K. A biomechanical regulatory model of periprosthetic tissue differentiation. J. Mater. Sci. Mater. Med. **8**, 785, 1997.

17. Kelly, D.J., Prendergast, P.J. Mechano-regulation of stem cell differentiation and tissue regeneration in osteochondral defects. J. Biomech. **38**, 1413, 2005.

18. Pauwels, F. Eine neue Theorie über den einfluss mechanischer Reize auf die Differenzierung der Stützgewebe, Z. Anat. Entwickl., 121, 478, 1960. Translated by Maquet, P., Furlong, R. as A new theory concerning the influence of mechanical stimuli in the differentiation of supporting tissues, in Biomechanics of the Locomotor Apparatus, 1980, 375-407.

19. Carter, D.R., Blenman, P.R., Beaupré, G.S. Correlations between mechanical stress history and tissue differentiation in initial fracture healing. J. Ortho. Res. **6**, 736, 1988.

20. Duda, G.N., Maldonado, Z.M., Klein, P., Heller, M.O.W., Burns, J. and Bail, H.. On the influence of mechanical conditions in osteochondral defect healing. J. Biomech. **38**, 843, 2005.

21. Loboa, E.G., Wren, T.A.L., Beaupré, G.S., Carter, D.R. Mechanobiology of soft tissue differentiation – a computational approach of a fiber-reinforced poroelastic model based on homogenous and isotropic simplifications. Biomech. Model. Mechanobiol. **2**, 83, 2003.

22. Claes, L.E., Heigele, C.A. Magnitudes of local stress and strain along surfaces predict the course and type of fracture healing. J. Biomech. **32**, 255, 1999.

23. Gómez-Benito, M.J., Garcia-Aznar, J.M., Kuiper, J.H., Doblaré, M. Influence of fracture gap size on the pattern of long bone healing: a computational study. J. Theor. Biol. **235**, 105, 2005.

24. Søballe, K., Hansen., E.S., B-Rasmussen, H., Jørgensen, P.H., Bunger, C. Tissue ingrowth into titanium and hydroxyapapite coated implants during stable and unstable mechanical conditions. J. Ortho. Res. **10**, 285, 1992.

25. Lacroix, D., Prendergast, P.J., Li, G., Marsh, D. Biomechanical model to simulate tissue differentiation and bone regeneration: application to fracture healing. Med. Biol. Eng. Comput. **40**, 14, 2002.

26. DiSilvestro, M. R., Suh, J. K. A cross-validation of the biphasic poroviscoelastic model of articular cartilage in unconfined compression, indentation, and confined compression. J. Biomech. **34**, 519, 2001.

27. Li, L.P., Buschmann, M.D., Shirazi-Adl, A. A fibril reinforced nonhomogeneous poroelastic model for articular cartilage: inhomogeneous response in unconfined compression. J. Biomech. **33**, 1533, 2000.

28. Bailon-Plaza, A., van der Meulen, M.C.H. A mathematical framework to study the effects of growth factor influences on fracture healing. J. Theor. Biol. **212**, 191, 2001.

29. Mauck, R. L., Nicoll, S. B., Seyhan, S.L., Ateshian, G. A., Hung, C. T. Synergistic action of growth factors and dynamic loading for articular cartilage tissue engineering. Tissue Eng. **9**, 597, 2003.

30. Shapiro, F., Koide, S., Glimcher, M. J. Cell origin and differentiation in the repair of full-thickness defects of articular cartilage. J. Bone Joint. Surg. **75A**, 532, 1993.

31. Metsäranta, M., Kujala, U. M., Pelliniemi, L., Österman, H., Heikki, A., Vuorio, E. Evidence of insufficient chondrocytic differentiation during repair of full-thickness defects of articular cartilage. Matrix Biol. **15**, 39, 1996.

32. Geris, L., Andreykiv, A., Van Oosterwyck, H., Vander Sloten, J., Van Keulen, F., Duyck J., Naert, I. Numerical simulation of tissue differentiation around loaded titanium implants in a bone chamber. Journal of Biomechanics, **37**, 763-769, 2004.

33. Akizuki, S., Mow, V.C., Müller, F., Pita, J.C., Howell, D.S., Manicourt, D. H. Tensile properties of human knee joint cartilage: I. Influence of ionic conditions, weight bearing, and fibrillation on tensile modulus. J. Ortho. Res. **4**, 379, 1986.

34. Maroudas, A, Bullough, P. Permeability of articular cartilage. Nature **219**, 1260, 1968.

35. Semple, J.L., Woolridge, N., Lumsden, C.J. In vitro, in vivo, in silico: Computational systems in tissue engineering and regenerative medicine. Tissue Eng. **11**, 341, 2005.

List of figures

Fig. 1. The mechano-regulation of tissue differentiation concept proposed by Prendergast *et al.* [14], and adapted by Lacroix and Prendergast [15] to account for bone resorption.

Fig. 2. Above: Sagittal section of right knee-joint, adapted from Gray's Anatomy, 20th edition. Below: Axi-symmetric finite element model of the chondyle of the knee with an osteochondral defect. Right: Finite element mesh illustrating loading and boundary conditions. Left: Defect (box) showing origin of mesenchymal stem cells (arrows).

Fig. 3. Comparison of the predicted patterns of tissue differentiation in an osteochondral defect during (a) spontaneous repair with no scaffold, and (b) repair in the presence of a homogenous scaffold. The defect region is highlighted by the box on the finite element mesh on the right hand side of the figure.

Fig. 4. Predictions of cell viability at a point at the centre of the articular surface of the defect throughout the simulation, with and without an implanted homogenous scaffold. Significant cell death is predicted during spontaneous repair, whereas the use of a scaffold prevents this.

Fig. 5. Influence of scaffold Young's modulus on the amounts of bone tissue, cartilage tissue and fibrous tissue predicted to form in the defect.

Fig. 6. Predicted patterns of tissue differentiation in 7 mm defect with and without an implanted homogenous scaffold.

Fig. 7. Influence of scaffold permeability on the amounts of bone tissue, cartilage tissue and fibrous tissue predicted to form in the defect.

Fig. 8. Variation in the Young's modulus and permeability of a computer optimised scaffold. (Note: 0-2 mm refers to the chondral phase of the scaffold, while 2-5 mm

refers to the bone phase of the scaffold. The Young's modulus is greatest in the chondral phase at the articular surface.)

Fig. 9. Predicted patterns of tissue differentiation in an osteochondral defect implanted with an optimized scaffold.

Fig. 10. The influence of varying either the Young's modulus or the permeability of the scaffold on the amounts of fibrous tissue predicted within the defect after 50 iterations of the simulation. (Note the log scale on the graph of permeability against fibrous tissue formation).

Tables

Table 1: Material Properties used in finite element model

	Granulation tissue	Fibrous tissue	Cartilage	Immature bone	Mature bone	Cortical bone
Young's modulus (MPa)	0.2	2	10	1000	6000	17000
Permeability ($m^4/Ns \times 10^{-14}$)	1	1	0.5	0.1	0.37	0.001
Poisson's ratio	0.167	0.167	0.167	0.3	0.3	0.3
Porosity	0.8	0.8	0.8	0.8	0.8	0.04
Solid compression modulus (MPa)	2300	2300	3400	13920	13920	13920
Fluid compression modulus (MPa)	2300	2300	2300	2300	2300	2300
Diffusion co-efficient (mm^2/iteration)	0.8	0.1	0.05	0.01	0.01	-

Table 2: Material properties of homogenous scaffold.

	Young's Modulus (MPa)	Permeability ($m^4/Ns \times 10^{-14}$)
Scaffold 1	1	1
Scaffold 2	5	1
Scaffold 3	10	1
Scaffold 4	20	1
Scaffold 5	50	1
Scaffold 6	10	0.5
Scaffold 7	10	0.1
Scaffold 8	10	0.05

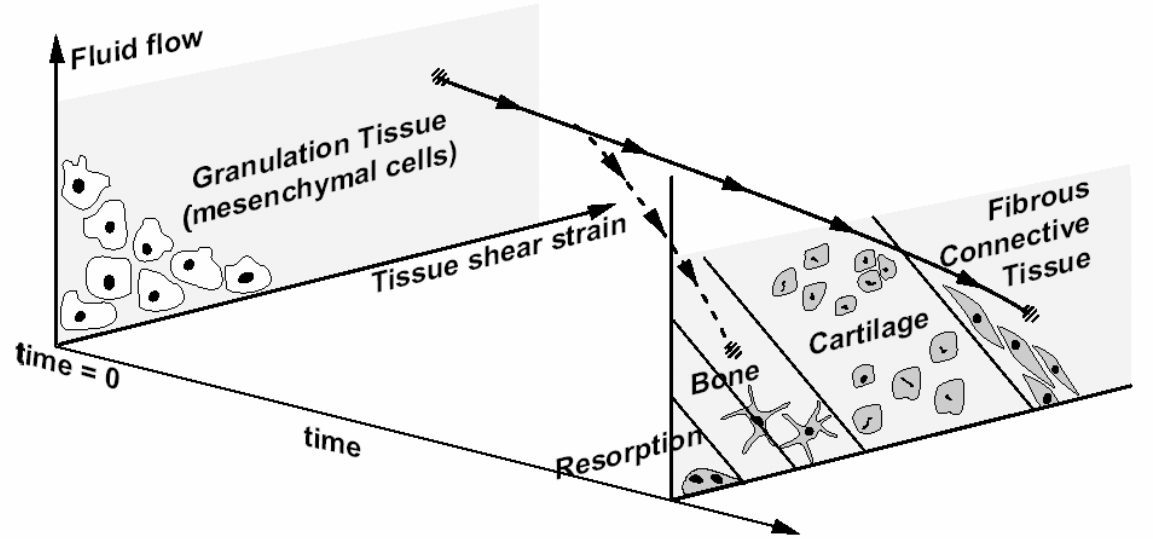

Fig. 1. The mechano-regulation of tissue differentiation concept proposed by Prendergast *et al.* [14], and adapted by Lacroix and Prendergast [15] to account for bone resorption.

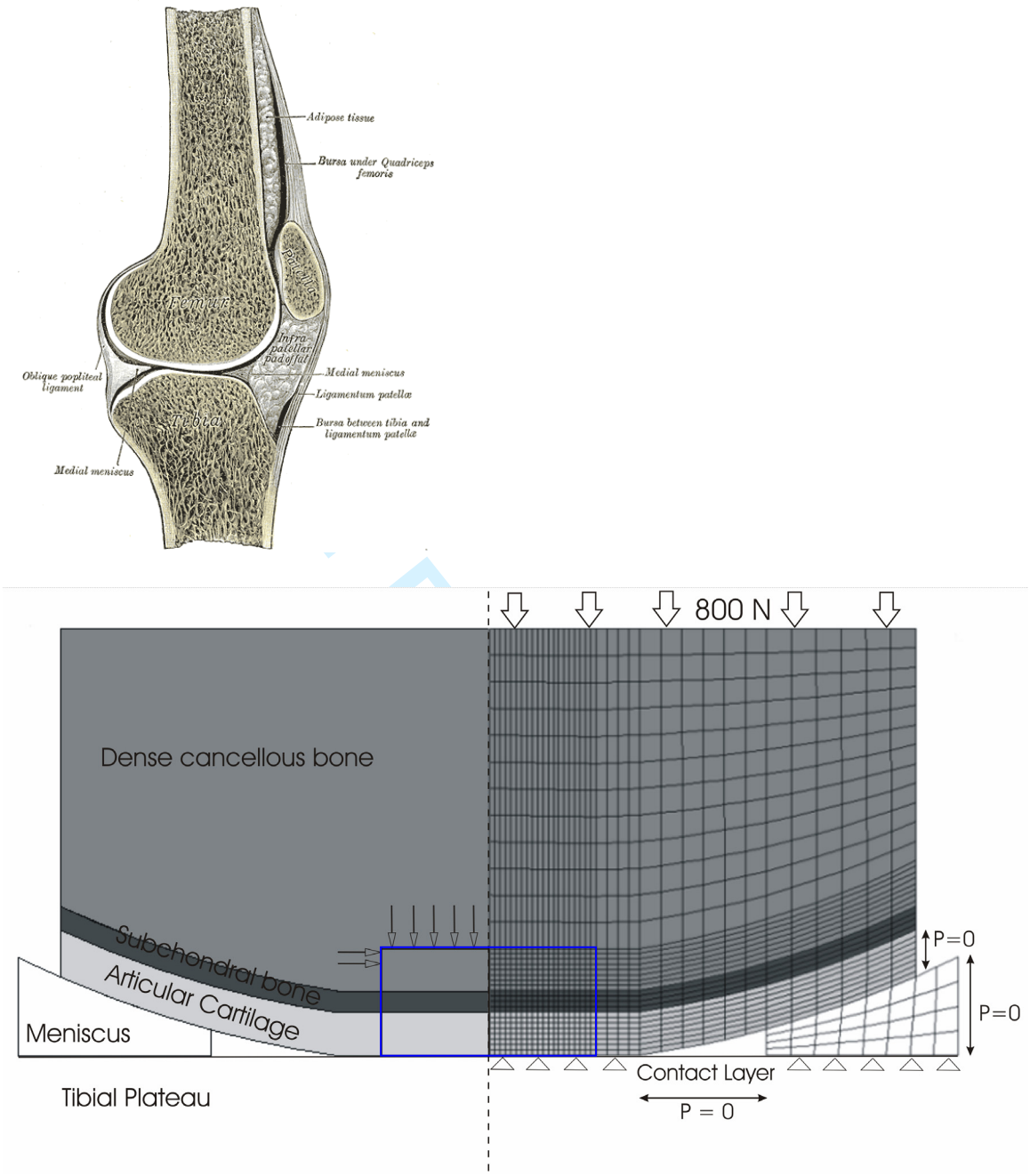

Fig. 2. Above: Sagittal section of right knee-joint, adapted from Gray's Anatomy, 20th edition. Below: Axi-symmetric finite element model of the chondyle of the knee with an osteochondral defect. Right: Finite element mesh illustrating loading and boundary conditions. Left: Defect (box) showing origin of mesenchymal stem cells (arrows).

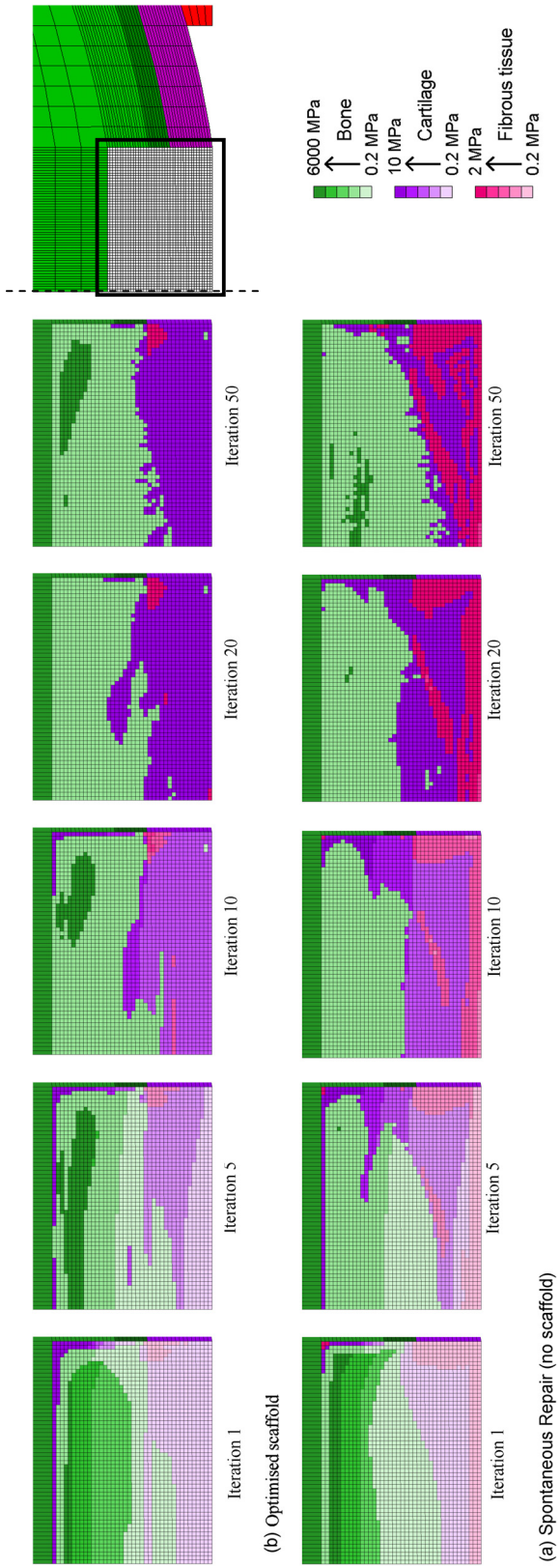

Fig. 3. Comparison of the predicted patterns of tissue differentiation in an osteochondral defect during (a) spontaneous repair with no scaffold, and (b) repair in the presence of a homogenous scaffold. The defect region is highlighted by the box on the finite element mesh on the right hand side of the figure.

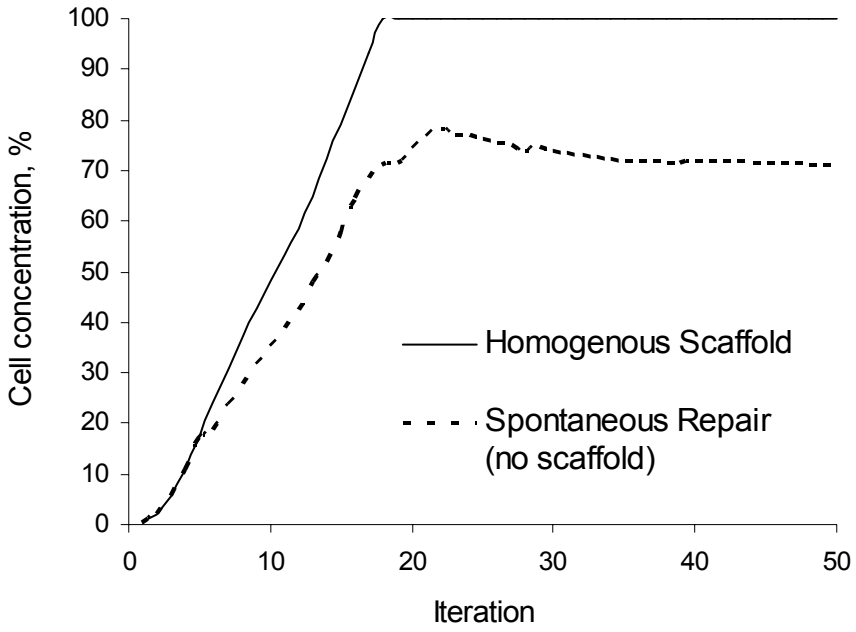

Fig. 4. Predictions of cell viability at a point at the centre of the articular surface of the defect throughout the simulation, with and without an implanted homogenous scaffold. Significant cell death is predicted during spontaneous repair, whereas the use of a scaffold prevents this.

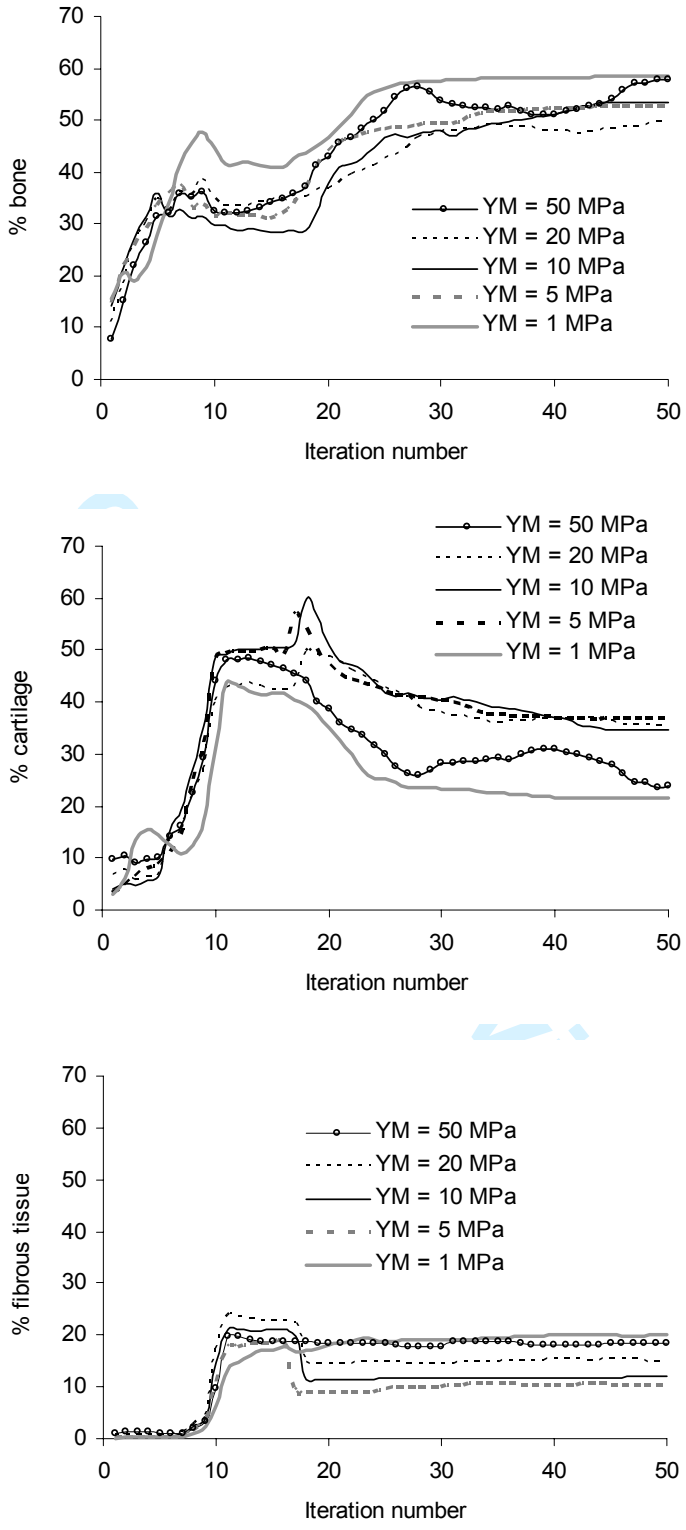

Fig. 5. Influence of scaffold Young's modulus on the amounts of bone tissue, cartilage tissue and fibrous tissue predicted to form in the defect.

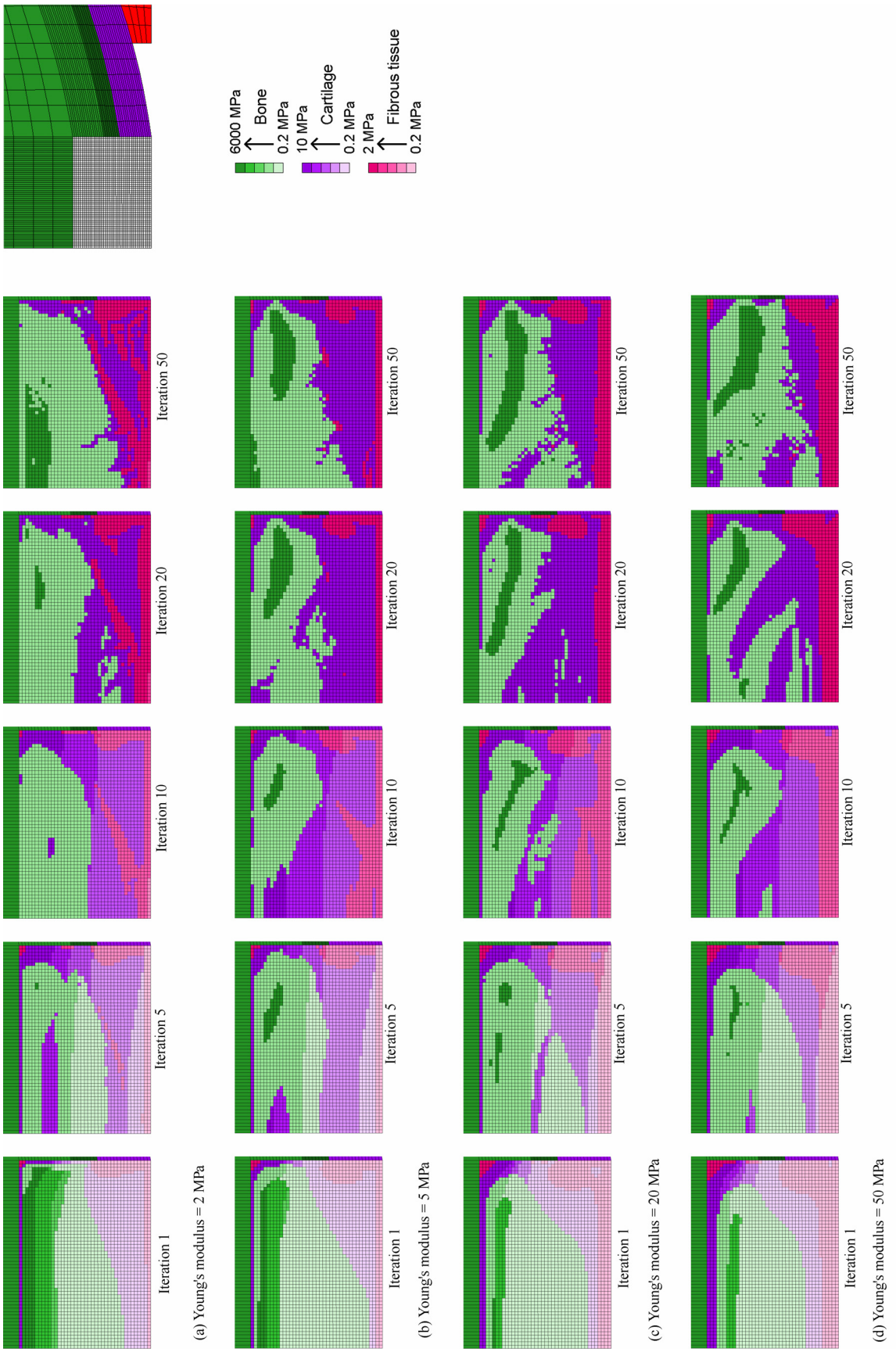

Fig. 6. Predicted patterns of tissue differentiation in 7 mm defect with and without an implanted homogenous scaffold.

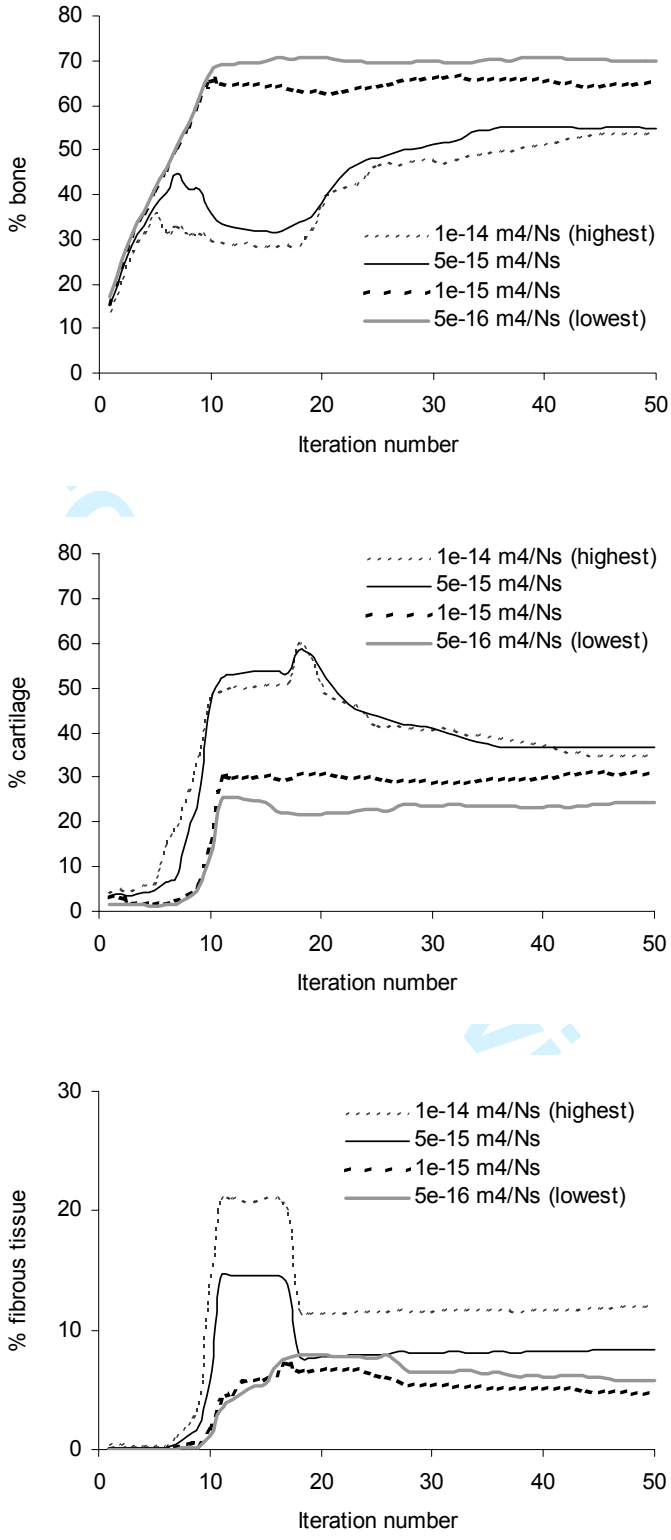

Fig. 7. Influence of scaffold permeability on the amounts of bone tissue, cartilage tissue and fibrous tissue predicted to form in the defect.

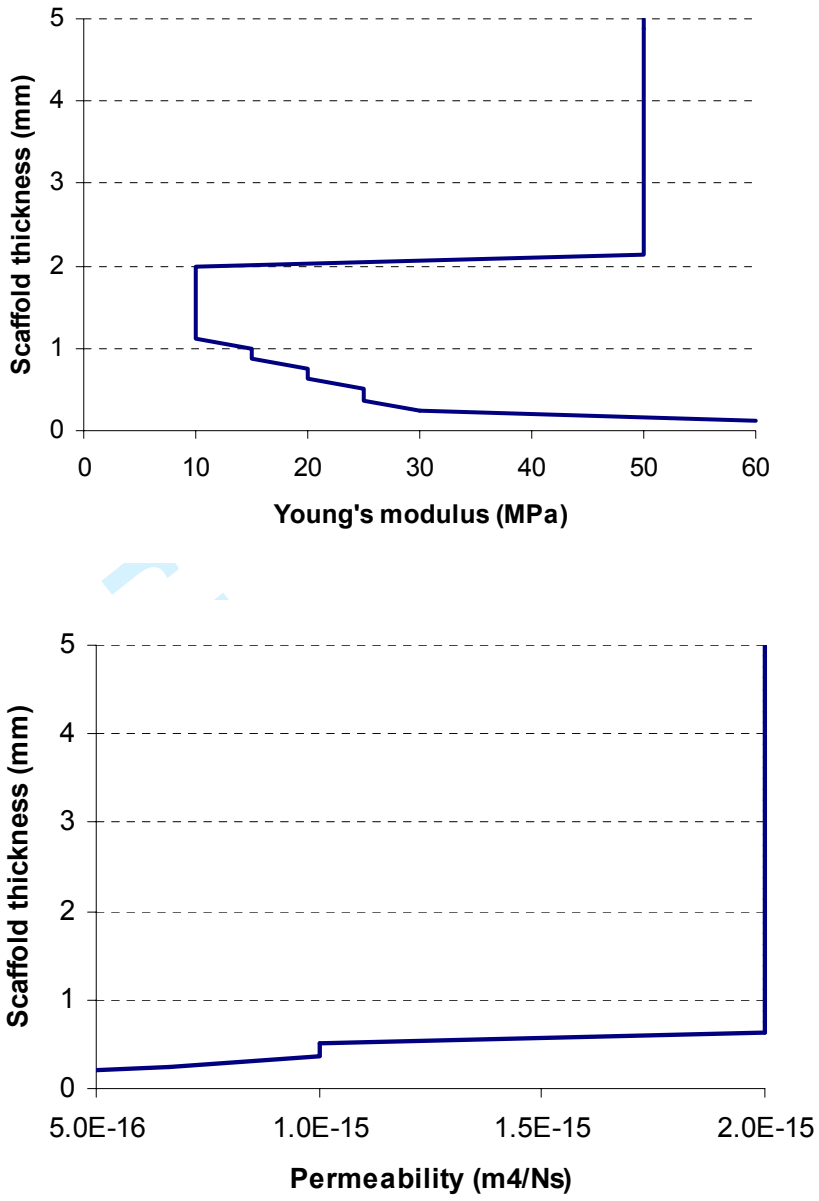

Fig. 8. Variation in the Young's modulus and permeability of a computer optimised scaffold. (Note: 0-2 mm refers to the chondral phase of the scaffold, while 2-5 mm refers to the bone phase of the scaffold. The Young's modulus is greatest in the chondral phase at the articular surface.)

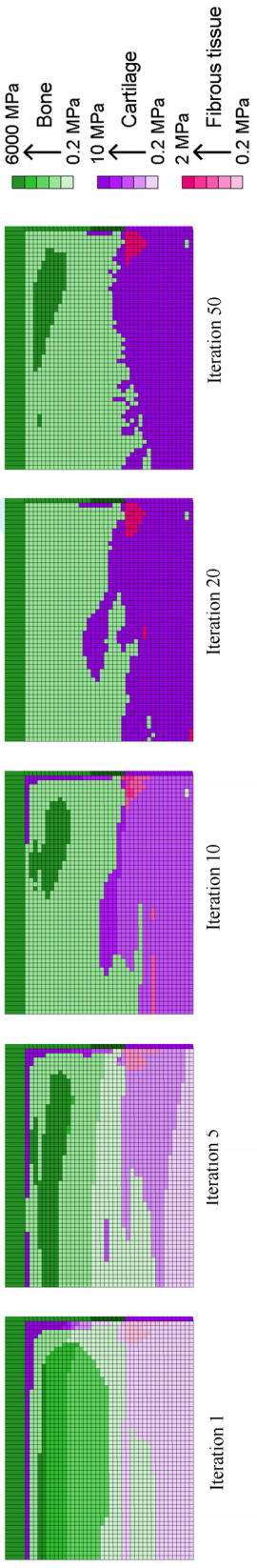

Fig. 9. Predicted patterns of tissue differentiation in an osteochondral defect implanted with an optimized scaffold.

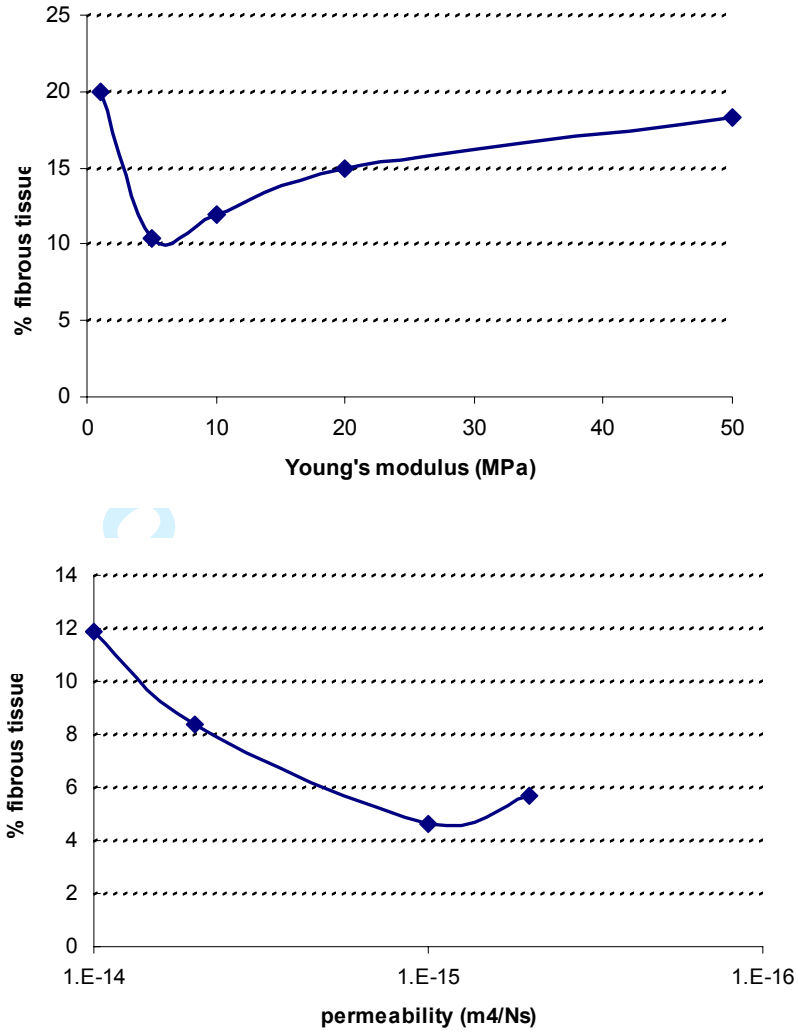

Fig. 10. The influence of varying either the Young's modulus or the permeability of the scaffold on the amounts of fibrous tissue predicted within the defect after 50 iterations of the simulation. (Note the log scale on the graph of permeability against fibrous tissue formation).